# Metal discrimination using multi-frequency electromagnetic induction

Ian J. Duckling*[a], Michael Chappell[a], John W. Cunningham[b]

[a]Thales Missile Electronics Ltd., Mountbatten House, RG21 4HJ, UK
[b]Sula Systems Ltd., Old Crown House, GL12 7AE, UK

## ABSTRACT

The use of Electromagnetic Induction (EMI) for land mine detection has been common for over six decades. Recent work in this field has focused on greater discrimination due to the difficulties in detecting mines amongst metal debris. The false alarm rate of such systems could be improved by the ability to discriminate between metal types. This paper presents initial results of a study into metal discrimination using a multi-frequency metal detector. Factors affecting the performance of such a system, including the choice of frequencies, and the mine size, orientation and metal composition are discussed. This work was carried out as part a UK MoD funded Programme.

Keywords: multi-frequency EMI, metal discrimination, mine detection, neural network classification

## 1. INTRODUCTION

Technologies for landmine detection have been the subject of much work over recent years. The scale of the landmine problem, for both military mobility and humanitarian causes has yet to be matched by a detection method that offers timely, reliable threat localisation. Metal detectors are synonymous with the task of landmine detection, and are used both in handheld and vehicular mounted configurations. An increasing number of landmines are constructed mainly of non-metallic materials, the only metal content being in the fuze. The occurrence of metallic debris of a similar size to fuze components, on or just below the soil surface, is frequent in post-conflict scenarios and so the false alarm rate of metal detectors can be high. The ability to discriminate between metal types has benefits in de-mining, since metallic clutter of certain types could be discounted as false alarms, potentially removing the need for further investigation.

A great deal of work has been conducted into metal discrimination using multi-frequency electromagnetic induction[1,2,3,4,5,6]. Much of this work has involved complex modelling of the underlying physical processes, and the development of purpose designed detector systems. The aim of this work is to evaluate the discrimination capability that could be provided by a Commercial-Of-The-Shelf (COTS) metal detector operating in a Continuous Wave Stepped Frequency (CWSF) mode. The study involves consideration of the size and orientation of metallic targets, and the contribution that such a system might make to a classification system.

The approach taken is practically based, with emphasis on experimentally observed results. However, some modelling of the phenomenology has been conducted in order to gain (mostly qualitative) theoretical predictions of the effects of metallic objects within the vicinity of the metal detector, and in order to establish some suitable metrics for the discrimination of metal types. This modelling is described in section 2.

Section 3 describes the experimental set-up used to gather data, and the process by which the data is handled. Section 4 presents results of the data gathering trials, and the resulting signal processing. Also described in section 4 is a classification method adopted for the analysis of the recorded data.

Section 5 contains a discussion of the work conducted in this study. Section 6 presents conclusions of the study, and suggests further work and improvements.

* ian.duckling@uk.thalesgroup.com; phone +44 (0) 1256 387659; fax +44 (0) 1256 387617; Thales Missile Electronics Ltd. Mountbatten House, Basing View, Basingstoke, Hampshire, RG21 4HJ, UK.



Detection and Remediation Technologies for Mines and Minelike Targets VII, J. Thomas Broach, Russell S. Harmon, Gerald J. Dobeck, Editors, Proceedings of SPIE Vol. 4742 (2002) © 2002 SPIE · 0277-786X/02/$15.00

## 2. THEORETICAL PREDICTIONS

This section is divided into three parts. First there is a description of the model developed for predicting the output of a CW metal detector. Second, there is a description of the targets used in this study, for both the theoretical modelling aspects, and the experimental data gathering. Finally, there is a brief analysis of the predicted results, with the aim of selecting suitable metrics for the discrimination of metals.

### 2.1 Metal detector model

Metal detector systems can be simulated using an analogue circuit equivalent model, and this approach is adopted in order to predict the performance of the system to be used. The system is considered to be a transformer, where the inductance characteristics of the coils, the loads in the circuit, and the flux leakage determine the induced signal in the secondary coil. The flux leakage is determined by the coupling coefficient ($k$) of the coils and the metallic target. The system is considered to be in free space, and so only the coils and target are of interest.

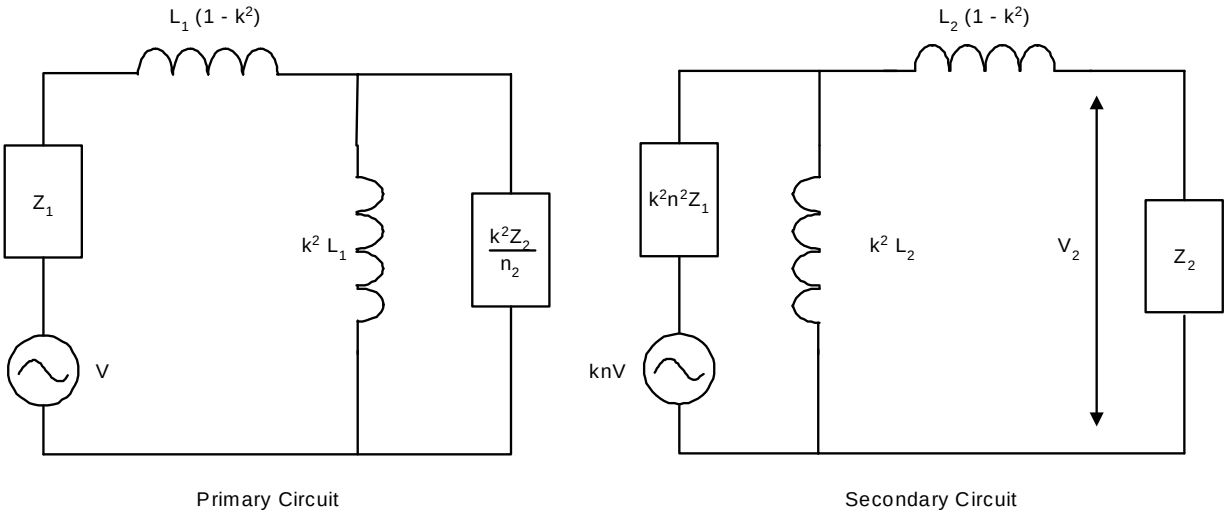


Figure 1 – Equivalent transformer circuit for metal detector system.

From the equivalent circuit in figure 1, it can be shown[7] that

$$V_2 = \frac{M}{\sqrt{L_1 L_2}} nV \left\{ \frac{Z_{IN}}{Z_1 + Z_{IN}} \right\} \left\{ \frac{Z_2}{Z_2 + j\omega\left(L_2 - M^2/L_1\right)} \right\} \tag{1}$$

$$M = k\sqrt{L_1 L_2} \tag{2}$$

Where $M$ is the mutual inductance, related to the coupling coefficient by equation (2), $n$ is the turns ratio, $\omega$ is the angular frequency, $L_1$ and $L_2$ are the self inductance of the primary and secondary circuits respectively, $Z_1$ and $Z_2$ are the impedance of the primary and secondary circuits and

$$Z_{IN} = j\omega\left(L_1 - \frac{M^2}{L_2}\right) + \frac{1}{\left(n^2 L_1 L_2 / M^2 Z_2\right) + \left(L_1 L_2 / j\omega M^2 L_1\right)} \tag{3}$$

is the input impedance of the equivalent transformer.

The Mutual inductance between the coils and the target is calculated using Neumann's formula[7,8].

$$M = \frac{\mu_0 \mu_r}{4\pi} \oint_{\Gamma_1} \oint_{\Gamma_2} \frac{d\mathbf{r}_i \cdot d\mathbf{r}_j}{\left|\mathbf{r}_i - \mathbf{r}_j\right|} \tag{4}$$

Where $\Gamma_1$ represents the current carrying loop of the coils, $\Gamma_2$ represents the induced current loop of the target, $\mathbf{r}_i$ and $\mathbf{r}_j$ are vectors from the origin to points on the coils and target respectively. $\mu_r$ is the relative permeability of the target. The integration is conducted numerically using Simpson's rule[9].

### 2.2 Targets

A number of targets were used in this study, and these are listed in table 1. Three targets (targets numbered 1 to 3 in table 1) were defined to ensure that a large return was present, such that any effects allowing the discrimination of these metals were present. The remainder of the targets were then used in order to test the discrimination ability of the system described in the following section (section 3).

| Target number | Target name / description | Target size (metallic component) | Metal type |
|---|---|---|---|
| 1 | Aluminium disc | ∅ 300 mm x 10 mm | Aluminium |
| 2 | Steel disc | ∅ 300 mm x 10 mm | Mild Steel |
| 3 | Brass disc | ∅ 300 mm x 10 mm | Brass |
| 4 | PMN (replica) | ∅ 10 mm x 60 mm | Stainless Steel |
| 5 | Cartridge case | ∅ 11 mm x 52 mm | Brass |
| 6 | Bottle cap | ∅ 30 mm x 6 mm | Aluminium |
| 7 | TMA-3 | ∅ 6 mm x 35 mm (3 off) | Aluminium |

Table 1 – Description of targets

(a) (b) (c)

Figure 2 – (a) PMN replica and (b) cartridge case (c) UTMA-3 fuse from TMA-3.

For the purpose of this simulation, the target is considered to be a flat metallic disc, corresponding to targets 1,2 and 3 in table 1. This simple shape has the advantage of allowing the mutual inductance expression derived from equation (4) to be expressed compactly in polar co-ordinates when the coils and target are co-axial. The metallic properties assumed for these targets are given in table 2, their size and shape is given in table 1.

| Target Number | Target name / description | Relative Permeability ($\mu_r$) | Conductivity (S/m) |
|---|---|---|---|
| 1 | Aluminium disc | 1 | $35.4 \times 10^6$ |
| 2 | Steel disc | 150 | $6.3 \times 10^6$ |
| 3 | Brass disc | 1 | $15.0 \times 10^6$ |

Table 2 – Properties of targets 1, 2 and 3.

### 2.3 Simulation results

Figure 3 shows the modelled In-phase and Quadrature-phase components of the resulting signal, $V_2$, for targets 1 and 2 at a distance of 150 mm. The diameter of the coils was 160 mm, and amplitude of the exciting signal was 9 V.

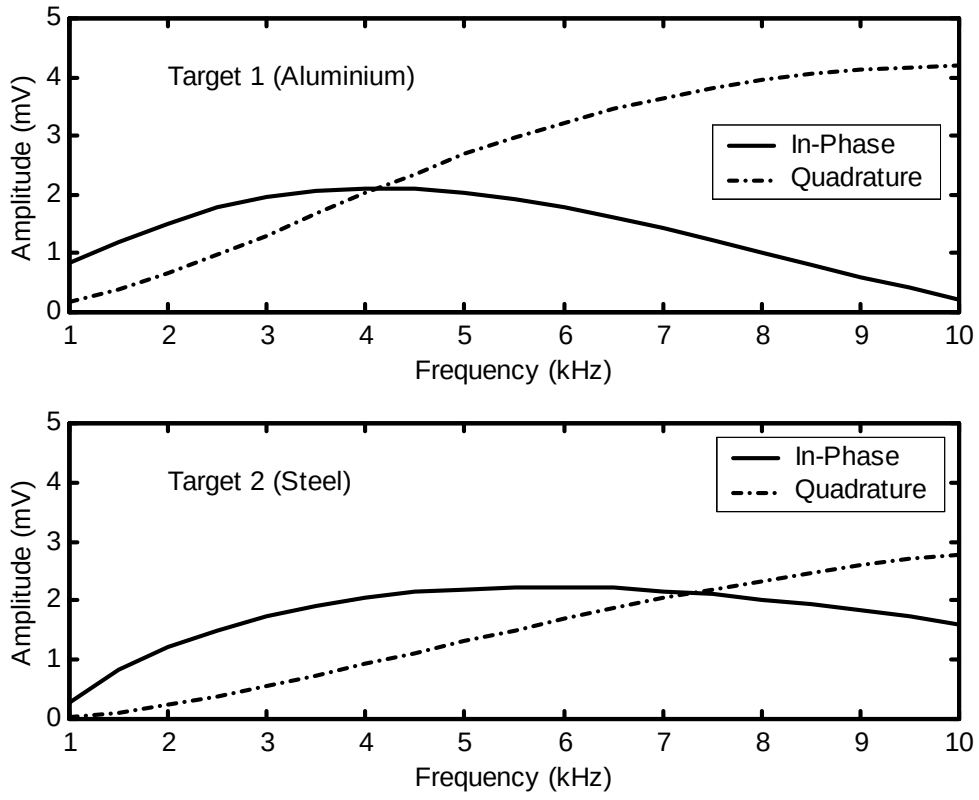


Figure 3 – Theoretical in-phase and quadrature components of the secondary circuit voltage $V_2$ for targets 1 and 2.

From the output of the model described by equations (1) to (4) several observations relating to the behavior of such a system are of note. Target conductivity becomes the dominant factor in the response as frequency increases; therefore the amplitude of the return from non-ferromagnetic metals (e.g. aluminium) increases with frequency. With a relative

permeability greater than unity, and conductivity lower than that of aluminium, target 2 (mild steel) exhibits lower signal amplitude compared with target 1 (aluminium) in the frequency range considered.

Previous work in this area has suggested that an object can be characterised by its frequency response, specifically in terms of the In-phase and Quadrature components of the induced signal[1,2,4]. Results of previous work have shown that the phase response is largely unaffected by target range[2], and the outcome of this simulation agrees with these findings, as shown in figure 4. Therefore, in characterizing an object, the shape of the two components of the response, and the frequency at which they are equal (the 'crossover' frequency) are believed to be sufficient for classification[3].

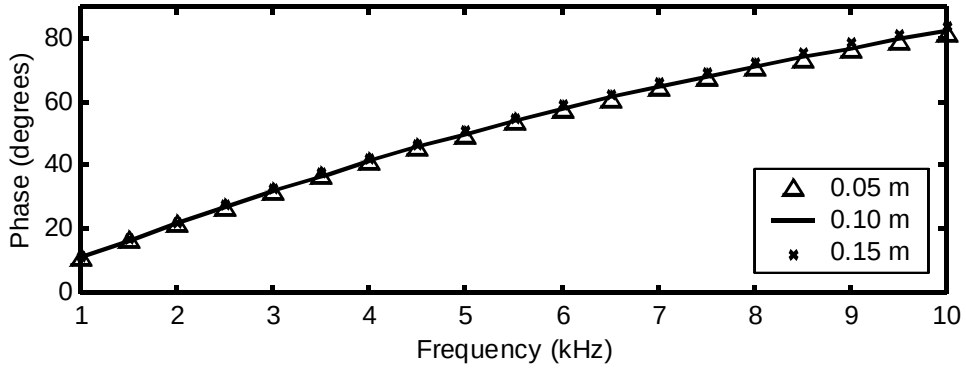


Figure 4 – Phase angle versus frequency for target 1 (aluminium), with target range as a variable

To this end a number of features describing the shape of the In-phase and Quadrature components are computed by fitting a polynomial to each in turn, using the least squares approach. The coefficients of these polynomials are then used as the input to the classification scheme described in section 4.2. Since the crossover frequency for both targets appears within the range 1 – 10 kHz, this spectrum is used in the experimental set-up described below.

## 3. EXPERIMENTAL SET-UP

This section describes the hardware and software used to collect and analyse multi-frequency induction data.

### 3.1 Hardware

The aim of this study is to determine the metal discrimination capability of a readily available, inexpensive, metal detector, and as such COTS hardware is used wherever possible. The detector electronics of a Viking 6DX system were removed, leaving just the 'head', which is interfaced to an IBM compatible PC. Figure 5 depicts the data gathering system constructed. The primary coil in the metal detector head is excited by a Software-Controlled Oscillator (SCO). The induced signal in the secondary coil is measured using a 16-bit analogue data acquisition PCI card in the host PC. The detector is excited with a stepped frequency sweep, programmable by the control software, but typically varied between 1 kHz and 10 kHz at 500 Hz intervals.

The induced signal is low-pass filtered prior to digitisation in order to minimise aliasing effects. The signal is digitised at a sufficiently fast rate to ensure that accurate phase recovery is possible. After each step change in frequency, and prior to the corresponding signal sampling, a short period is allowed to ensure transient effects have subsided. Approximately 10 ms of data is digitised for each frequency, and the resulting sweep time (for the range given above) is 0.5 seconds.

The metal detector head is mounted on a 2-axis (horizontal) scanning frame to allow accurate positioning of the detector head over targets which can either be suspended in free space, or laid in soil bins of non-metallic construction.

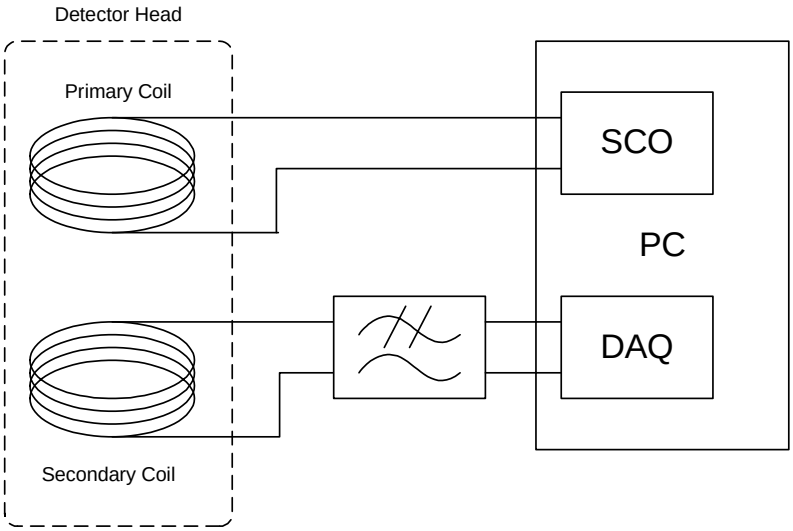


Figure 5 – System diagram of metal detector set-up

### 3.2 Software

All processing of the collected data is performed in software, allowing flexibility of the scheme adopted. Figure 6 shows the processing scheme implemented in order to extract In-phase and Quadrature components of the induced signal.

In order to ensure that the frequency response extracted is entirely due to the target, both the amplitude and phase must be corrected to eliminate the effects of the acquisition circuit (namely the anti-aliasing filter).

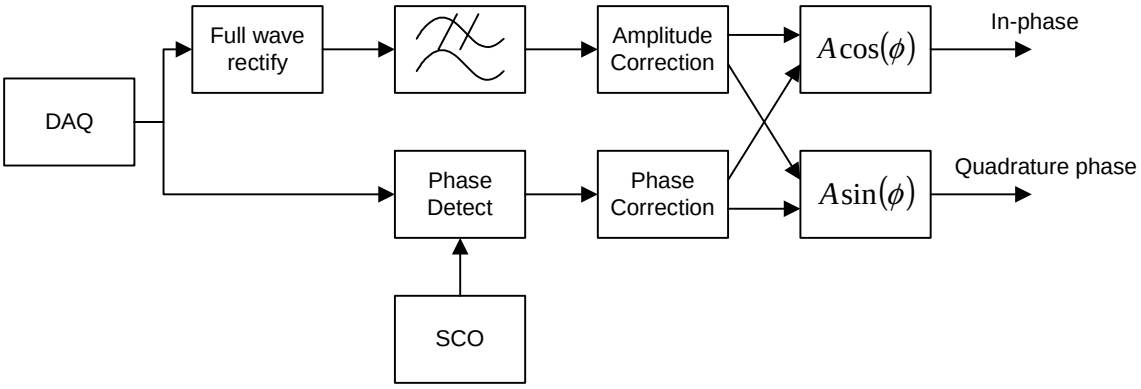


Figure 6 – Processing scheme adopted for extraction of In-phase and Quadrature components.

## 4. RESULTS

This section presents results of the data gathering conducted with the set-up described in section 3. These results are compared with the output of the system model described in section 2. A scheme for object classification is then presented, and its output evaluated.

### 4.1 Comparison with modelled results

Processing of the collected data using the scheme described in section 3 allows a direct comparison of the measured and modelled results. Figure 7 shows the modelled and measured In-phase and Quadrature components of the induced signal for target 1 (aluminium).

Whilst the results in figure 7 show a general agreement between modelled and measured results, there are clearly some differences. On inspection, these differences are caused by uncertainties in the circuit properties, both in terms of the parameters used in the equivalent circuit model in section 2.1, and the phase and amplitude correction process described in section 3.2. In particular, since the mutual inductance of the coils is very small (of the order of $\mu$H), reactive components of circuit loads that were not considered in section 2 will cause an increasing discrepancy between modelled and measured results as the frequency rises.

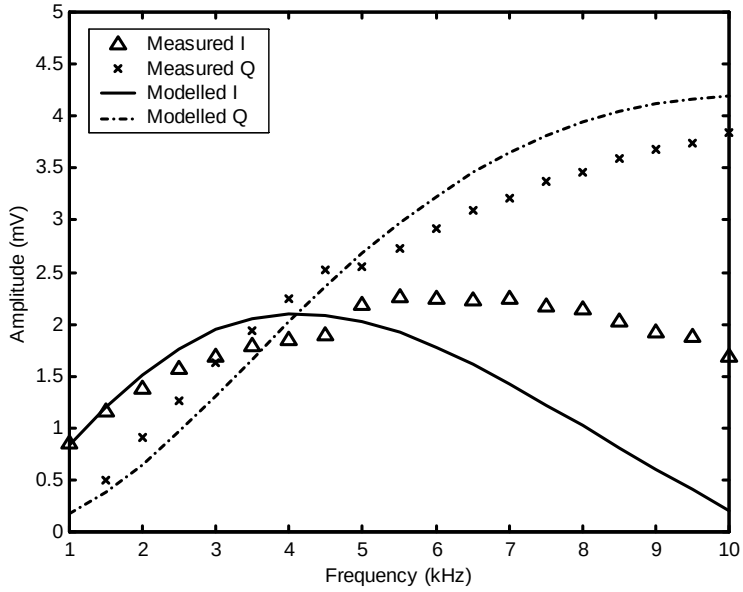


Figure 7 – Comparison of modelled and measured results for target 1 (aluminium).

### 4.2 Classification of targets

As discussed in section 2.3, the shape of the In-phase and Quadrature components of the measured signal can be represented by the coefficients of a polynomial function that has been fitted to the data using the least squares method. The task remains to classify the targets based on these coefficients.

Initially, a quadratic function is fitted to each component of the measured signal, giving a total of six values for each data set. A feature vector, **a**, is then constructed, where *f* is the frequency in Hz, and:

$$\begin{aligned} \mathbf{a} &= \{a_1, a_2, a_3, a_4, a_5, a_6\} \\ In-phase &= a_1 f^2 + a_2 f + a_3 \\ Quadrature &= a_4 f^2 + a_5 f + a_6 \end{aligned} \tag{5}$$

The error associated with these approximations was found to be small, and as the results presented below indicate, this feature vector appears to be sufficient for the classification task.

A Multi-Layer Perceptron (MLP) was selected for the classification task, since a neural network has certain advantages over other techniques for this application. In particular, ease of implementation was a deciding factor, since there is no need to specify prior relationships between the feature vector elements, as would be required for a classical Bayesian approach. Previous experience with MLPs would suggest that with a suitable quantity of training data the network could be trained to provide a classification scheme robust to changes in target range, orientation and off-axis position. The MLP constructed has two hidden layers, the first hidden layer containing ten neurons, and the second containing five. The output of the single neuron in the output layer represents the target type, as listed in table 1.

The Levenberg-Marquardt algorithm[10] is used to train the network. Figure 8 (a) shows the output of the network, after training for classification of targets 1 and 2. The training data consisted of ten feature sets for targets 1 and 2, co-axially positioned in free space, with range varying between 50 mm and 150 mm. The test data sets (figure 8 (a) shows a sample of these results) were collected with the targets placed in coarse sand. The range was varied as for the training data set, however the orientation of the targets was varied (with a maximum angle of 40° to the horizontal) and the co-axial limitation was removed (maximum 100 mm offset between coil and target centers). The solid line in figure 8 (a) depicts the true type of the target, i.e. data sets 1 and 2 were measurements taken with target 2, sets 3 to 5 with target 1, and so on. The circles represent the output of the neural network, which is a continuous variable. Variation in the network output from the discrete target type indicates a non-perfect match. The output shown in figure 8 is rounded to the nearest integer to give a classification decision.

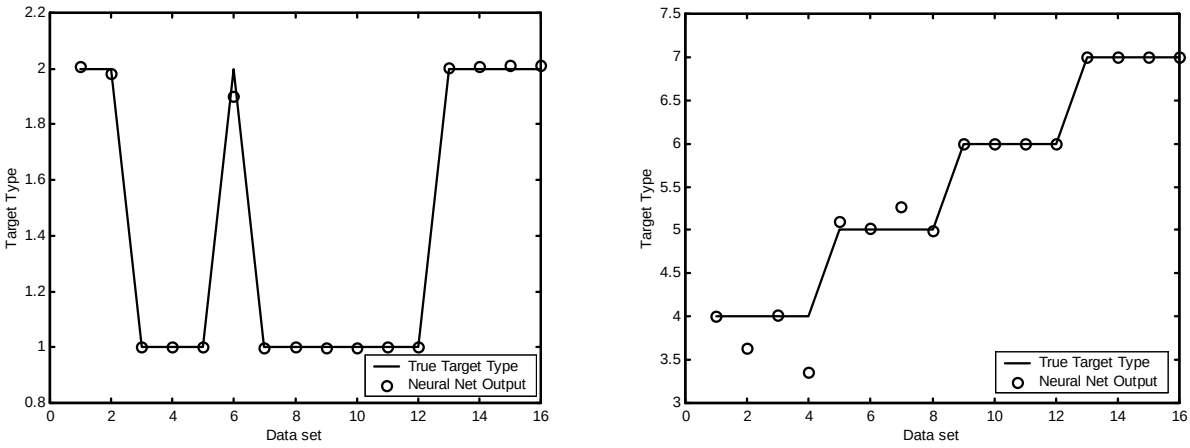


Figure 8 – Network performance (a) network output and true target type for targets 1 and 2 (b) for targets 4 to 7.

For the 16 data sets shown, and indeed for all data sets used to test the network for targets 1 and 2, the application of the decision threshold yielded a perfect classification record. This is largely unsurprising, since, although the geometry of the targets is identical, the metallic properties are quite different (one is ferrous, the other is not!). The network was unable, however, to successfully distinguish between targets 1 and 3 (aluminium and brass respectively).

The network was then trained, in a fashion similar to that described above, for targets 4 to 7. The results of the network classification are presented in figure 8 (b) for a sample of the test data.

Table 3 provides the correct classification rates achieved for targets 4 to 7. These figures were obtained from 860 data sets, containing 200 or more instances of each target.

| Target Type | Target Description | Correct Classification Rate (%) |
|---|---|---|
| 4 | PMN | 80.5 |
| 5 | Cartridge case | 69.0 |
| 6 | Bottle cap | 100.0 |
| 7 | TMA-3 | 98.0 |

Table 3 – Classification rates for targets 4 to 7

## 5. DISCUSSION

As shown in figure 8 (a), the implemented system can discriminate between ferrous and non-ferrous objects of the same size and shape. More usefully, however, the system is capable, with a moderate degree of success, to classify targets with relatively small metal content at a range of distances, and with some variation of orientation and horizontal position.

The results of both the system simulation and the experimental measurements would suggest that the phase response of the targets is largely independent of range, and so the classification success of the scheme adopted depends on the variation due to orientation and horizontal position, the difference in properties of the target's metallic components, and the ability of the system to measure these differences.

This, then, would explain the system's inability to differentiate between targets 1 and 3. The targets have the same size and shape, and the properties of the metals from which they are made provide insufficient contrast to allow successful classification when the orientation or horizontal position changes.

The task would therefore seem to be more one of object discrimination than metal discrimination, since, apart from the ferrous / non-ferrous property, the response is principally dependent on the object's size and shape.

The data given in table 4 relating to the metal types that are likely to be found in post-conflict scenarios (both mines and clutter) would suggest that discriminating between ferrous and non-ferrous metals, whilst useful, could not alone be used to reduce the false alarm rate. However, as part of a multi-sensor system this information could be combined with other data in order to build-up a clearer picture in order to derive a more definitive evaluation of the objects detected.

| Mine Type / Object | Metal type |
|---|---|
| PFM-1 ("Butterfly" AP) | Aluminium |
| TMA-4 | Aluminium |
| POM-2S | Steel |
| PMN | Steel |
| PMA-2 | Aluminium |
| Drinks can | Steel / Aluminium |
| Bottle cap | Steel / Aluminium |
| Food packaging | Aluminium / Tin |

Table 4 – Metallic constituents of mines and battlefield debris

Whilst the performance achieved with this study appears to be favourable, there are several limitations that should be noted.

- The number of targets used was far smaller than the wide range of objects a de-miner is likely to encounter. With a greater number of objects to classify, it is inevitable that the boundaries between some will be unclear. However,

with good intelligence relating to the threats likely to be encountered, the number of target types in the search need not be vast.

- This work included no consideration of the soil conditions in the area surrounding the targets. Measurements were made in free space (air), and in (dry) coarse sand. Many studies have shown the effects of soil type and water content on the performance of metal detectors, and these will have an effect on the ability to discriminate objects..

## 6. CONCLUSIONS

A SFCW EMI system has been constructed from inexpensive COTS hardware for the evaluation of multi-frequency data. This study has shown that, as a potential method of enhancing a conventional metal detector, multi-frequency EMI data can provide some further cues in the discrimination of mines in a real battlefield scenario.

The limitations of the work undertaken have been discussed, and these naturally lead to considerations for future work. Two areas of particular interest are the investigation of the effects of soil properties on the discrimination ability, and further data gathering to assess the robustness of the classification algorithm as the number of target types increases.

## ACKNOWLEDGMENTS

The work described in this paper was funded under a UK MoD programme. The opinions expressed in this paper are solely those of the authors, and do not represent UK Government policy. The authors gratefully acknowledge the managements of Thales Missile Electronics Ltd and Sula Systems Ltd for permission to publish this paper.

## REFERENCES

1. Carin, L. Baum, C. E.; “Wideband Time- and Frequency-Domain EMI: Phenomenology and Signal Processing”; Department of Defense, UXO Center of Excellence, Technical Report; 36 pages; 2001.
2. Bruschini, C., Sahli, H.; “Phase angle based EMI object discrimination and analysis of data from a commercial differential two frequency system”; Proceedings of the SPIE AeroSense 2000, Detection and Remediation Technologies for Mines and Minelike Targets; Vol. 4038; pp ; 2000.
3. Gao, P., Collins, L., Garber, P. M., Geng, N., Carin, L.; “Classification of Landmine-Like Metal Targets Using Wideband Electromagnetic Induction”; IEEE Transactions on GeoScience and Remote Sensing; Vol. 38 No. 3; pp1352-1361; 2000
4. Won, I. J., Keiswetter, D. A., Bell, T. H.; “Electromagnetic Induction Spectroscopy for Clearing Landmines”; IEEE Transactions on Geoscience and Remote Sensing; Vol. 39, No. 4; pp703-709; 2001
5. Won, I. J., Keiswetter, D. A., Fields, G. R. A., Sutton, L. C.; “GEM-2: A New Multifrequency Electromagnetic Sensor”; JEEG, Vol. 1, Issue 2; pp129-137; 1996.
6. Won, I. J., Keiswetter, D. A., Hanson, D. R., Novikova, E., Hall, T. M.; “GEM-3: A Monostatic Broadband Electromagnetic Induction Sensor”; JEEG Volume 2, Issue 1; pp53-64; 1997.
7. Grant, I. S., Phillips, W. R.; Electromagnetism; pp314; John Wiley & Sons; Chichester; 2001
8. Bueno, M., Assis, A. K. T.; “Equivalence between the formulas for Inductance calculation”; Canadian Journal of Physics; Vol. 75; pp357-362; 1997
9. Jeffery, A.; Essentials of Engineering Mathematics; pp318; Chapman & Hall; London; 1995
10. Hagan, M. T., Menhaj, M.; “Training feedforward networks with the Marquardt algorithm”; IEEE Transactions on Neural Networks; Vol. 5, No. 6; pp989-993; 1994.